Effects of nozzle geometry on direct injection diesel engine combustion process

R. Payri, F.J. Salvador, J. Gimeno, J. de La Morena

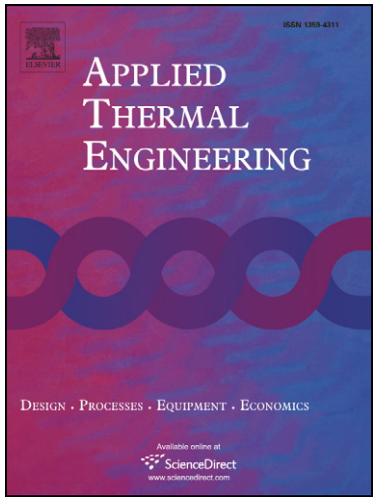

Effects of nozzle geometry on direct injection diesel engine combustion process

R. Payri, F.J. Salvador, J. Gimeno, J. de la Morena

PII: S1359-4311(08)00421-3
DOI: 10.1016/j.applthermaleng.2008.10.009
Reference: ATE 2641

To appear in: *Applied Thermal Engineering*

Received Date: 19 February 2008
Revised Date: 17 September 2008
Accepted Date: 27 October 2008

Please cite this article as: R. Payri, F.J. Salvador, J. Gimeno, J. de la Morena, Effects of nozzle geometry on direct injection diesel engine combustion process, *Applied Thermal Engineering* (2008), doi: 10.1016/j.applthermaleng.2008.10.009

EFFECTS OF NOZZLE GEOMETRY ON DIRECT INJECTION DIESEL ENGINE COMBUSTION PROCESS

R. Payri (*), F. J. Salvador, J. Gimeno, J. de la Morena

CMT-Motores Térmicos, Universidad Politécnica de Valencia

Camino de Vera s/n, E-46022 Spain.

(*) Corresponding author:

Dr. Raul Payri, rpayri@mot.upv.es

CMT-Motores Térmicos, Universidad Politécnica de Valencia

Camino de Vera s/n, E-46022 Spain.

Telephone: +34-963879658

FAX: +34-963877659

ABSTRACT

The aim of the current article is to link nozzle geometry, and its influence on spray characteristics, with combustion characteristics in the chamber. For this purpose, three 6-hole sac nozzles, with different orifices degree of conicity, have been used. These nozzles had been geometrically and hydraulically characterized in a previous publication, where also a study of liquid phase penetration and stabilized liquid length in real engine conditions has been done. In the present work, CH and OH chemiluminescence techniques are used to thoroughly examine combustion process. CH-radicals are directly related to pre-reactions, which take place once the fuel has mixed with air and it has evaporated. On the other hand, OH-radicals data provide information about the location of the flame front once the combustion has begun. The analysis of all the results allows linking nozzle geometry, spray behaviour and combustion development. In particular, CH-radicals have shown to appear together with vapour spray, both temporally and in their location, being directly related to nozzle characteristics. Additionally, analysis of ignition delay is done form OH measurements, including some correlations in terms of chamber properties, injection pressure and nozzle diameter.

KEY WORDS:

Diesel, nozzle geometry, liquid length, chemiluminescence, combustion.

NOMENCLATURE

A	Constant in the ignition delay correlation that represents E_A/R.
C_a	Contraction coefficient
C_{mv}	Fuel mass concentration needed in the spray axis to get complete evaporation
C_v	Velocity coefficient
D_{eff}	Outlet effective diameter of a nozzle orifice.
D_{eq}	Equivalent diameter of a nozzle orifice. Defined as $D_{eq} = D_o\sqrt{\frac{\rho_l}{\rho_a}}$
D_i	Inlet diameter
D_o	Outlet diameter
EA	Activation energy
ET	Energizing time
K	Constant used in the ignition delay correlation.
k-factor	Nozzle conicity. Defined as $kfactor = 100 \cdot \frac{D_i - D_o}{L}$
K_p	Constant in LL analysis, including the effect of cone angle
L	Nozzle length
LL	Liquid Length
n-m-l	Coefficients used in the ignition delay correlation.
P_{back}	Backpressure.
P_{inj}	Injection pressure.
SOE	Start of Energizing
SOI	Start of Injection
t_{mv}	Time for a fuel parcel in the axis of a stationary spray to reach a concentration equal to $C_{mv.}$

T	Temperature in the engine injection chamber.
TDC	Top Dead Center
u_{eff}	Effective velocity at the outlet orifice, defined as $u_{eff} = C_a^{1/2} \cdot D_o$
u_{th}	Theoretical velocity, obtained from Bernoulli equation as $u_{th} = \sqrt{\frac{2\Delta P}{\rho_l}}$

Greek symbols:

ΔP	Pressure drop, $\Delta P = P_{inj} - P_{back.}$
ρ_a	Ambient density.
ρ_l	Fuel density.
λ	Wave length
τ	Time elapsed from the start of the injection to start of combustion (ignition delay).

1. INTRODUCTION

Pollutant emission reduction is currently considered to be one of the most important targets of our society. Legislation about pollution coming from vehicles is getting more and more restrictive, so that research is focused to understand physical processes involved in the engine behaviour.

One of the most important subjects in these studies on Diesel engines is the behaviour of fuel once it is injected in the combustion chamber, and its interaction with air. In these terms, it is well known that nozzle geometry and cavitation strongly affect to evaporation and atomization processes of fuel. The study of these phenomena has been the aim of previous studies in the literature [1]-[8].

Another method to understand what is happening in the engine is analyzing combustion process directly. Several optical techniques have been used by other authors [9]-[11] to analyze combustion process in the chamber. Soot flame visualization and CH/OH chemiluminescence are the most important techniques referred in literature.

CH-radicals are formed in low temperature reactions. For this reason, they are assumed as an indicator of pre-reactions, which are the first step for the combustion process, once fuel is evaporated [12].

OH- is an intermediate species in high temperature reactions. This implies that OH-radicals are located in the flame front, where vaporized fuel reaches the highest temperatures. Because of this characteristic, OH appearance is often used to determine ignition delay [12], [13].

The aim of the current article is to link nozzle geometry, and its influence on spray characteristics [14],[15],[16],[17], with combustion development in the chamber. For this purpose, three 6-hole sac nozzles, with different orifices degree of conicity, have been used.

These nozzles had been geometrically and hydraulically characterized in [1], where also a study of stabilized liquid length in real engine conditions has been done. In the present work, CH and OH chemiluminescence techniques are used to thoroughly examine combustion process. The analysis of the results allows linking nozzle geometry, spray behaviour and combustion development.

The paper is structured in four sections. First of all, experimental facilities and methodology are described, paying special attention to image acquisition and processing. A new contour mapping technique, which allows seeing the spatial and temporal evolution of combustion simultaneously, is also introduced. After this, a representation of the experimental results obtained is presented, including a review of some interesting ideas coming from previous studies about stabilized liquid length. In the following section, some analysis about results already presented will be made. In this sense, CH radicals will be related to liquid length results, while OH provides information about ignition delay, including some correlations for it in terms of chamber conditions and injection parameters. Finally, some general conclusions concerning to chemiluminescence results will be established.

2. EXPERIMENTAL METHODOLOGY

All the experimental tests were done using a standard common rail injection system, including a high pressure pump and a rail, able to regulate pressure inside. Fuel used was Repsol CEC RF-06-99. Main properties of this fuel are reported in Table 1.

2.1 Nozzles

In order to make a study in terms of nozzle geometry influence, three 6-hole sac nozzles have been used. Despite Bosch flow number (defined as $\frac{\dot{m}_f}{\sqrt{\Delta P}}$) is the same for the three

nozzles, they are made with different degrees of conicity, represented by *k*-factor. Inlet diameter is fixed to approximately 175 µm for all of them. This group of nozzles includes one cylindrical and two convergent geometries. Complete information about their geometry, including inlet and outlet diameters (obtained using the methodology described in [18]), as well as *k*-factor, are shown in Table 2.

2.2 CH and OH chemiluminescence

A single-cylinder two stroke engine is used for combustion visualization studies. The experimental set up is equipped with an optical accessible cylinder head, which contains a cylindrical combustion chamber, as shown in Figure 1. More information about the engine characteristics can be found in [19].

CH and OH radicals can be visualized because they emit light intensity in a well defined wavelength band (λ) of the emitted light spectrum. For this reason, using a proper optical filter, emission corresponding to each species can be discerned from the total amount of light coming from combustion process. In this study, CH is acquired using a filter for λ between 375 and 405 nm, while OH correspond to the range 305-315 nm.

Nevertheless, the total amount of light emitted at these frequencies is small, so an intensified ICCD camera has to be used. In this case, LaVision-Dinamight camera is chosen, giving a resolution of 512 x 512 pixels.

Intensification gain level was fixed for each chemiluminescence technique, so that results from different tests can be compared. Two aspects were taken into account: on the one hand, it is important for the current study to get information about the first appearance of radicals; on the other hand, camera sensor saturation must always be avoided as much as possible. Finally, high levels of gain were selected for the acquisition process (99 % in case of CH radicals,

95% for OH radicals), cutting it off if extended saturation appears. Exposure time for image acquisition was fixed to 20 µs in all the tests.

Due to velocity limitations of the camera, only one image is taken at each injection process. In order to get information about CH- and OH-radicals evolution along the engine cycle, the camera trigger is delayed properly depending on injection pressure (a time step of 30 µs between photographs for an injection pressure of 30 MPa, and 20 µs for 80 MPa and 160 MPa). For statistical analysis purpose, 3 repetitions are taken at each time step.

Table 3 shows the experimental matrix. There are three different injection pressures (30, 80 and 160 MPa) operating under four engine conditions, determined by pressure and temperature at *TDC* (Top Dead Center). These conditions provide also four different chamber densities, specified in the table. Energizing time (ET), as well as in previous liquid spray studies, is chosen in order to reach stabilized liquid length conditions. For this reason, ET values were 2 ms for injection pressures of 30 MPa and 80 MPa, and 1 ms for the injection pressure of 160 MPa.

2.3 Image Processing

Images obtained have been analyzed with a purpose-made software. Each image is divided in sectors, corresponding to each nozzle orifice. Once each sector is isolated, software analyzes intensity in terms of radial position, calculating a mean value in the whole sector. An example of information given by software is shown in Fig. 2, where intensity coming from OH-radicals visualization at a specific time instant and for a single sector has been plotted. Result belongs to nozzle 2, chamber conditions of 7 MPa and 950 K, and an injection pressure of 80 MPa. As it can be seen from the figure, the evolution of radial intensity is a non-

symmetric bell-shape distribution, where the maximum amount of intensity is placed near the chamber wall. This result is also confirmed in the photograph.

Using the complete sequence of images, time analysis can be also done. In fact, if information from previous figure is integrated in terms of radius, a single value of intensity for each sector and image (time step) is obtained. In this way, evolution of intensity in terms of time, including all the radial positions, can be observed, as shown in Fig. 3. With this kind of graphs, it is possible to determine when the phenomena studied (CH or OH chemiluminescence) starts, and also when the maximum level of intensity is placed.

Nevertheless, in order to get a better understanding of combustion process, it is interesting to analyze simultaneously time of appearance and radial position. According to this idea, 2-D contour maps (Fig. 4) have been chosen as the optimal way of representation. In this figure, the measured intensity (emitted by OH radicals) is represented by means of a grey scale labeled contour map. This type of graphs allows the simultaneous representation of spatial (in **Y**-axis) and temporal (**X**-axis) data obtained from each test point to be performed.

In the example presented in Figure 4, distribution of different levels of OH intensity can be observed. In this figure, two photographs taken at different time instants and coming from visualization experiments are compared with the information represented in the graph. As it can be seen, intensity levels in the first photograph are much lower, because combustion process is at first stages. Instead of this, after a delay of approximately 0.3 ms, OH concentration is higher, being located nearer the chamber wall. Nevertheless, it is important to remark that contour map represents mean values of all the chamber sectors and all the repetitions.

3. EXPERIMENTAL RESULTS

3.1. Previous liquid-length penetration results

Liquid spray in evaporative conditions was previously studied for the presented nozzles. As described in [1], assuming that vaporization process is controlled by mixing and using turbulent spray theory for a fuel parcel in a quasi – steady spray, the following expression is obtained for the stabilized liquid length:

$$LL = \frac{K_p^2 \cdot \left(\frac{1}{4}\cdot\frac{\pi}{4}\cdot C_a\right)^{\frac{1}{2}} \cdot D_o \cdot \rho_l^{\frac{1}{2}}}{C_{mv} \cdot \rho_a^{\frac{1}{2}}} = \frac{K_p^2 \cdot \left(\frac{1}{4}\cdot\frac{\pi}{4}\cdot C_a\right)^{\frac{1}{2}} \cdot D_{eq}}{C_{mv}} \quad (1)$$

Where K_p is a constant that includes the dependence on spray cone angle, C_a is a contraction coefficient [7], D_o the outlet diameter of the nozzle, D_{eq} the equivalent diameter, ρ_a and ρ_l densities of air and fuel respectively, and C_{mv} is the value of fuel mass concentration in the axis at which liquid fuel is totally evaporated, due to the entrainment of warm air. It can be seen that *LL* shows to be proportional to D_{eq}.

For a given engine condition, the parameters C_{mv} , ρ_a , ρ_l are fixed, so that variations in spray penetration are justified in terms of outlet diameter, contraction coefficient (which depends on cavitation regime) or spray cone angle (included in K_p).

An example of liquid spray behaviour, summarizing the most important results extracted from [1], is shown in Figure 5, where the liquid length penetration is depicted against the start of Energizing (S.O.E). From the experimental results, it is observed that cylindrical nozzle (N3) provided the highest values of LL at low injection pressures (30 MPa and 80 MPa), due to its higher diameter and the absence of cavitation ($C_a \approx 1$). On the other hand, when comparing the two conical nozzles, no clear differences are shown. In this case, there are

opposite effects from outlet diameter, higher for N2, and contraction coefficient, for which N3 shows higher values.

Nevertheless, when increasing injection pressure, cavitation was more severe in the cylindrical nozzle, and the effect of diameter was compensated by the decrease of C_a. For this reason, the three nozzles have quite similar values of liquid length in the tests performed.

Nozzles can also be compared in terms of vaporizing time. Following a similar analysis, this expression can be found for the time to mix and vaporize:

$$t_{mv} \propto \frac{K_p^2 \cdot \frac{1}{4} \cdot \left(\frac{\pi}{4} \cdot C_a\right)^{\frac{1}{2}} \cdot D_{eq}}{C_{mv}{}^2 \cdot C_v \cdot u_{th}} \tag{2}$$

Where t_{mv} represents the time that a particle of a quasi-steady diesel spray needs to mix with hot air and vaporize completely, C_v a velocity coefficient and u_{th} is the theoretical velocity (defined using Bernoulli's equation between the inlet and the outlet of the nozzle orifice, as described in [1]) . Values of t_{mv} are obtained using values of effective velocity (u_{eff}), already obtained experimentally in [1] for all the nozzles combining injection rate and spray momentum measurements.

Figure 6 shows t_{mv} values for two different chamber conditions, and for the three nozzles. In general terms, nozzle with higher outlet diameter (N3) shows also the higher time to mix and vaporize. Conical nozzles (N1 and N2) perform with similar behaviour, as it happened with stabilized liquid-length. As it was seen in liquid length analysis, difference between cylindrical and convergent nozzles becomes almost negligible at high injection pressures, due to the effect of cavitation phenomena in N3.

Nevertheless, it is important to underline in this case that only a qualitative comparison between nozzles can be made in terms of t_{mv} because it is not an experimental measurement

and values of C_{mv} are not known. This is the reason why the unit of t_{mv} in Fig. 6 is arbitrary (a/u).

3.2. Chemiluminescence technique

Images were taken using the ICCD camera with the proper filter. Using the procedure described in section 2.3, contour maps are shown in Figure 7 for the two kinds of visualization and the three nozzles involved in the study.

Furthermore, in order to extract as much information as possible from the experiments, the liquid phase penetration is plotted as circles together with chemiluminescence results. This comparison is also needed to contrast that time and position of appearance is consistent with previous results. Additionally, position of maximum intensity at each time step is overlapped as a continuous line.

In the following section, analysis of CH- and OH-radicals will be done separately. Nevertheless, when comparing the contour maps from both measurements for the operating points presented in Fig. 7, several general comments can be done:

- Delay between the SOI and CH and OH appearance is shown in the figure. In order to get a clearer idea about the tendencies shown by both of them, values for all the conditions used in this study are plotted in figure 8. As it can be seen, behaviour of CH and OH appearance is similar to what it has been seen for *LL* and t_{mv}. Nozzle 3 (cylindrical nozzle), which has the highest diameter, also shows the highest values of time of appearance, while conical nozzles show shorter delay between *SOI* and pre-reactions. Delay between CH and OH appearance mainly depends on chamber conditions, and not on injection parameters, because it is controlled by chemical reactions.

- Geometry of contour maps (Figure 7) is clearly different in the two cases. CH-radicals are directly related to vapour phase spray development. That is the reason why pre-reactions contour maps show a particular triangle shape, being strongly affected by penetration curve slope at the beginning. Instead of this, OH-radicals show a more squared contour map.

4. ANALYSIS OF COMBUSTION

4.1. Pre-reactions study.

As it has been said before, CH-radicals are an indicator of low temperature reactions that only could take place once the fuel is completely mixed with air and vaporized. As it can be seen in Fig.7, first appearance of CH-radicals seems to be located next to the liquid spray.

It is supposed that CH-radicals should appear beyond the position of the stabilized liquid length. Nevertheless, CH intensity is detected before liquid phase penetration reaches *LL* value. The explanation to that behaviour relies on the fact that fuel vaporization begins first in the lateral boundary of the spray, and so, before the stabilization of liquid length.

In order to make a deeper analysis about CH-radicals and spray penetration, theoretical time of mixing and vaporized (t_{mv}, already studied) and time of appearance of pre-reactions are compared in Figure 9. These values are relative to Nozzle 3 behaviour, in order to make non-dimensional analysis. It can be seen that, in almost all the cases, relative values are lower than 1, which indicates that cylindrical nozzle needs higher times both for vaporizing and appearing CH radicals. In the same sense, Nozzle 2 shows the lowest relative values for the two parameters presented in the plot. These facts indicate the relationship between vaporization and pre-reactions.

Anyway, it is not instantaneous that a fuel particle gets evaporated and generates CH-radicals. There is a chemical delay necessary to perform this process. This delay depends on chamber conditions, and becomes almost negligible when temperature and pressure in the combustion chamber are high.

4.2. Ignition delay correlation.

As it was introduced in previous sections, OH chemiluminescence can be used to define ignition delay, because OH-radicals production are a result of the high temperature reactions present in the flame front.

Several authors have tried to perform semi-empirical equations for predicting ignition delay as a function of engine conditions. Ramos [20] and Heywood [21] made a review about empirical expressions for predicting the ignition delay.

In some of them, the authors arrived to Arrhenius-like expressions (Stringer [22], Wolfer [23], Hiroyasu [24]) as described in the following formula:

$$\tau = K \cdot {P_{back}}^{n} \cdot \exp\left(\frac{E_A}{R \cdot T}\right) \quad (3)$$

Where τ is the delay between start of injection and start of combustion, E_A the activation energy and T and P_{back} represent temperature and pressure in the combustion chamber.

Previous cited authors consider pressure and temperature existing at TDC for their analysis. Others, like Watson [25], have used the same Arrhenius type equation but using mean values of P_{back} and T during the combustion delay. Finally, some authors (Kadota [26], Shipinski [27]) used Livengood and Wu integration [28] as a way to take into account pressure and temperature variations during the delay period.

In a similar study, Pischinger [29] included the effect of injection pressure, which has a lot to do with mixing and vaporizing and, consequently, on ignition delay. For this reason, he proposed the following expression:

$$\tau = K \cdot {P_{back}}^{n} \cdot \exp\left(\frac{E_A}{R \cdot T}\right) \cdot {P_{inj}}^{m} \quad (4)$$

Based on previous expression, and taking into account the experimental measurements, an ignition delay correlation was searched. For this purpose, P_{back} and T were and temperature at Top Dead Center. All the pressures will be included in MPa, time of combustion in ms, and temperature in K. In order to simplify the statistical process, E_A/R was reduced in a common term, called A.

From statistical analysis, all the variables included have shown to be significant in the correlation. Marquardt algorithm arrives to the correlation presented in Table 4.a, with *R-square* of around 95 %. Intervals of each coefficient are also given with a confidence level of 95 %. Predicted vs. observed data are shown in Figure 10.

The final expression of the ignition delay can be divided in two effects: chemical delay, taken into account by chamber conditions (P_{back} and T); and physical delay, which would be controlled by ΔP (P_{inj}-P_{back}). Moreover, it is obvious that combustion depends on previous physical phenomena, that include air-fuel mixing and vaporization, and also on chemical phenomena, related to the reactions involved in the process.

As it can be seen, the searched correlation does not include effects of nozzle geometry (diameter), in spite of its tested importance on mixing and vaporizing process. Nevertheless, this expression can be useful for predicting ignition delay for a given combustion chamber condition and when effective diameter is not known.

In order to quantify the effect of the effective diameter on the ignition delay, a second correlation was searched including this effect. It is supposed that nozzle geometry affects only

to mixing and vaporizing processes, while chemical reactions velocities are independent of effective diameter. As it has been described in Section 3.1, where the parameter t_{mv} was introduced, time to mix and vaporize depends linearly on diameter, as shown in equation 2. Extrapolating this behaviour to the current analysis, the following correlation was proposed:

$$\tau = K \cdot {P_{back}}^{n} \cdot \exp\left(\frac{A}{T}\right) \cdot {P_{inj}}^{m} \cdot D_{eff} \quad (5)$$

Where D_{eff} is effective diameter, defined as $C_a^{1/2} \cdot D_o$.

Results from the statistical analysis are presented in Table 4.b. Effective diameter exponent was fixed to 1, keeping the dependency observed for this variable in the theoretical analysis. The rest of the coefficients were found very similar to those obtained in the first correlation. Also high value of R-square is obtained which indicates that assumption about diameter effect on ignition delay is accurate.

Finally, effect of *k-factor* can be taken into account. For this purpose, a correlation presented in eq.(6)(is searched:

$$\tau = K \cdot {P_{back}}^{n} \cdot \exp\left(\frac{A}{T}\right) \cdot {P_{inj}}^{m} \cdot D_{eff} \cdot (1 + kfactor)^{l} \quad (6)$$

Coefficients obtained for this correlation are included in Table 4.c. As it can be seen, correlation accuracy increases from that obtained in the previous correlation. This fact implies that *k-factor* has a significant effect on ignition delay.

5. CONCLUSIONS

The aim of this paper has been to check the influence of nozzle geometry on combustion process under real engine conditions.

For this purpose, CH- and OH- chemiluminescence techniques have been used. Images were taken with an intensified CCD camera in an optically accessible engine, reproducing conditions of a real engine, in three nozzles, differing on *k-factor*. Results are compared with previous geometric and hydraulic characterization, as well as liquid phase spray measurements, previously made in the same engine and for the same conditions.

In order to get a better comprehension of CH- and OH- appearance along the engine cycle, a particular representation technique is described and used. This technique allows getting simultaneous information of radial distribution and temporal appearance of radicals.

CH-radicals have shown to be clearly influenced by spray behaviour (air-fuel mixing and vaporizing process). In fact, CH appear together to spray vapour, after a short delay, depending on chamber conditions. Remarking this fact, theoretical time to mix and vaporize (t_{mv}) has been compared with CH-appearance, being clearly correlated.

OH- radicals can be considered as a measurement of ignition delay. Good agreement between CH- and OH- appearance is observed, in general terms. This is explained taking into account that combustion involves physical processes, related with the delay of CH-appearance, and chemical reactions, whose velocity mainly depends on chamber conditions.

Finally, several Arrhenius-kind correlations are searched, based on previous studies. Influence of chamber conditions (related with chemical processes) and injection pressure (due to mixing and vaporizing) are observed. Additionally, correlations including effective diameter and *k-factor* terms are also studied. Although their accuracy decreases respect to correlation that only includes chamber conditions and injection pressure, these correlations are useful in order to quantify the effect of nozzle geometry on ignition delay.

ACKNOWLEDGMENTS

This research has been funded in the frame of CAVI-Spray project; reference GV06/060 from Generalitat Valenciana. The authors would like to thank Mr. José Enrique del Rey from CMT-Motores Térmicos, Universidad Politécnica de Valencia, for providing the experimental measurements.

REFERENCES

[1] Payri, R., Salvador, F. J., Gimeno, J., Zapata, L. D., Diesel nozzle geometry influence on spray liquid-phase fuel penetration in evaporative conditions, Fuel 87 (2007): 1165-1176.

[2] Martinez-Martinez, S., Sanchez-Cruz, F.A., Riesco-Avila, J.M., Gallegos-Munoz, A., Aceves, S.M., Liquid penetration length in direct diesel fuel injection. Applied Thermal Engineering, 28, Issue: 14-15, (2008): 1756-1762.

[3] Suh, H.K., Lee, C.S., Effect of cavitation in nozzle orifice on the diesel fuel atomization characteristics. International Journal of heat and fluid flow, 29(4) (2008): 1001-1009.

[4] Payri, R., Molina, S., Salvador, F.J., Gimeno, J. A study of the relation between nozzle geometry, internal flow and sprays characteristics in diesel fuel injection systems KSME International Journal, 18(7) (2004): 1222-1235.

[5] Kent, J. C., Brown, G. M. Nozzle exit flow characteristics for square-edged and rounded inlet geometries, Combust. Sci. Technol 30 (1983): 121-132.

[6] Kampmann, S., Dittus, B., Mattes, P., Kirner, M., The influence of hydro grinding at VCO nozzles on the mixture preparation in a DI Diesel engine, SAE Paper 960867 (1996).

[7] Payri, R., García, J. M., Salvador, F. J., Gimeno J., Using spray momentum flux measurements to understand the influence of Diesel nozzle geometry on spray characteristics, Fuel 84 (2005): 551-561.

[8] Goney, K. H., Corradini, M. L., Isolated effects of ambient pressure, nozzle cavitation and hole inlet geometry on Diesel injection spray characteristics, SAE Paper 2000-01-2043 (2000).

[9] Ganipa, L. C., Andersson, S., Chomiak, J., Combustion characteristics of Diesel sprays from equivalent nozzles with sharp and rounded inlet geometries, Combust. Sci. and Tech. 175 (2003): 1015-1032.

[10] Siebers, D., Higgins, B., Flame lift-off on direct-injection Diesel sprays under quiescent conditions, SAE Paper 2001-01-0530

[11] Musculus, M. P. B., Effects of the in-cylinder environment on diffusion flame lift-off in a DI Diesel engine, SAE Paper 2003-01-0074

[12] Dec, J.E., Espey, C., Chemiluminescence imaging of auto-ignition in a DI Diesel engine. SAE paper 982685

[13] Costa, M., Vaglieco, B.M., Corcione, F.E., Radical species in the cool-flame regime of diesel combustion: a comparative numerical and experimental study. Experiments in Fluids (2005) 39: 512–524

[14] Lee, C.S., Lee. K.H., Reitz, R.D., Park, S.W., Effect of split injection on the macroscopic development and atomization characteristics of a diesel spray injected through a common-rail system. Atomization and Sprays, 16(5), 2006: 543-562.

[15] Kastengren, A., Powell, C.F. Spray density measurements using X-Ray radiography. Proceedings of the institution of mechanical engineers part D-Journal of automobile engineering, 221 (D6) (2007): 653-662.

[16] Desantes, JM; Payri, R; Pastor, JM; Gimeno, J Experimental characterization of internal nozzle flow and diesel spray behavior. Part I: Nonevaporative conditions. Atomization and Sprays, 15 (5) (2005): 489-516

[17] Benajes, J; Payri, R; Molina, S; Soare, V Investigation of the influence of injection rate shaping on the spray characteristics in a diesel common rail system equipped with a piston amplifier. Journal of fluids engineering-transactions of the ASME, 127(6) (2005): 1102-1110

[18] Macián, V., Bermúdez, V., Payri, R., Gimeno, J., New technique for determination of internal geometry of a Diesel nozzles with the use of silicone methodology, Exp. Techniques 27(2003): 39-43.

[19] Bemúdez, V., García, J.M., Juliá, E., Martínez, S., Engine with Optically Accessible Cylinder Head: a research tool for injection and combustion processes, SAE Paper 2003-01-1110.

[20] Ramos, J., Internal combustion engine modelling, Hemisphere publishing corporation, ISBN 0-89116-157-0, 1989

[21] Heywood, J., Internal combustion engine fundamentals, Mc. Graw-Hill, ISBN 0-07-028637-X, 1988

[22] Stringer, F.W., Clarke, A.E., Clarke, J.S., The spontaneous ignition of hydrocarbon fuels in a flowing system", Proc. Instn Mech Engrs., vol. 184, 1969-1970.

[23] Wolfer, H.H., Ignition lag in Diesel engines, VDI-Forschungsheft 392, 1938; translated by Royal Aircraft Establishment, Farnborough Library No. 358, UDC 621-436.047, 1959

[24] Hiroyasu, H., Kadota, T., Arai, M., Supplementary coments: fuel spray characterization in Diesel engines, Combustion modeling in Reciprocating Engines, pp. 369-408, 1980.

[25] Watson, N., Transient performance simulation and analysis of turbocharged Diesel engines, SAE paper 910338 (1981).

[26] Kadota, T., Hiroyasu, H., Ohya, H., Ignition delay of fuel droplet in high pressure gaseous environments, Trans. of JSME, Vol. 41, No. 348, p. 2475 (1975).

[27] Shipinski, J., Meyers, P.S., Uyehara, O.A., A spray droplet model for Diesel combustion, Inst. Mech. Engineering 184 Part 3J (1969-1970)

[28] Livengood, J.C., Wu, P.C., Correlation of autoignition phenomena in internal combustion engines and rapid compression machines. Fifth Symposium (international) on Combustion, 347 (1955).

[29] Pischinger, F., Reuter, V, Scheid, E., Self ignition of Diesel sprays and its dependence on fuel properties and injection parameters, J. of Eng. For Gas Turbine and Power 110 (1988): 399-404.

LIST OF TABLES

FIGURE CAPTIONS

Table 1. Physical and chemical properties of Repsol CEC RF-06-99 fuel.

Test	Unit	Result	Uncertainty	Methodology
Density at 15ºC	**Kg/m^3**	**843**	**±0.2**	**EN ISO 12185/96**
Viscosity at 40ºC	**mm^2/s**	**2.847**	**±0.42**	**EN ISO 3104/99**
Volatility				
65% distillated at	**ºC**	**294.5**	**±3.7**	**EN ISO 3405:01**
85% distillated at	**ºC**	**329.2**	**±3.7**	
95% distillated at	**ºC**	**357.0**	**±3.7**	
Cetane Number	**------**	**51.52**	**± 2.5**	
Cetane Index	**------**	**49.6**	**± 0.51**	
Calorific Value				
Higher Calorific Value	**MJ/kg**		**45.58**	**ASTM D-240/02**
Lower Calorific Value	**MJ/kg**		**42.78**	**ASTM D-240/02**
Fuel molecular composition		**$C_{13}H_{28}$**		

Table 2. Real orifice nozzle geometry characterization by silicone methodology.

Nozzle	**D_i [μm]**	**D_o [μm]**	**k-factor**
1	175	155	2
2	176	160	1.6
3	175	175	0

Table 3. Engine test matrix conditions.

Injection		**Chamber conditions**			**Acquisition**	
Inj. P. [MPa]	E.T. [ms]	P. at TDC [MPa]	T at TDC [K]	Density (Kg/m3)	Δt (μs)	Repetitions
30	2	5	950	18	30	3
30	2	5	800	22	30	3
30	2	7	950	26	30	3
30	2	7	800	30	30	3
80	1	5	950	18	20	3
80	1	5	800	22	20	3
80	1	7	950	26	20	3
80	1	7	800	30	20	3
160	1	5	950	18	20	3
160	1	5	800	22	20	3
160	1	7	950	26	20	3
160	1	7	800	30	20	3

Table 4: Coefficients of ignition delay correlation

a. Correlation without diameter			b. Including diameter		c. Including k-factor	
EXP.	**FIT**	**Confidence Interval**	**FIT**	**Confidence Interval**	**FIT**	**Confidence Interval**
k	0.26	[0.18, 0.34]	1.64	[0.73, 2.56]	1.35	[0.84, 1.86]
n	-0.89	[-1.04, -0.74]	-0.91	[-1.10, -0.73]	-0.89	[-1.09,-0.695]
A	2510.9	[2227, 2795]	2509	[2165, 2853]	2509.4	[2155,2843]
m	-0.14	[-0.17, -0.11]	-0.12	[-0.16, -0.08]	-0.097	[-0.14,-0.052]
l	-	-	-	-	0.095	[0.033,0.157]
R-Squared= 94.84 %			R-Squared= 92.48 %		R-squared = 92.92%	

Figure 1

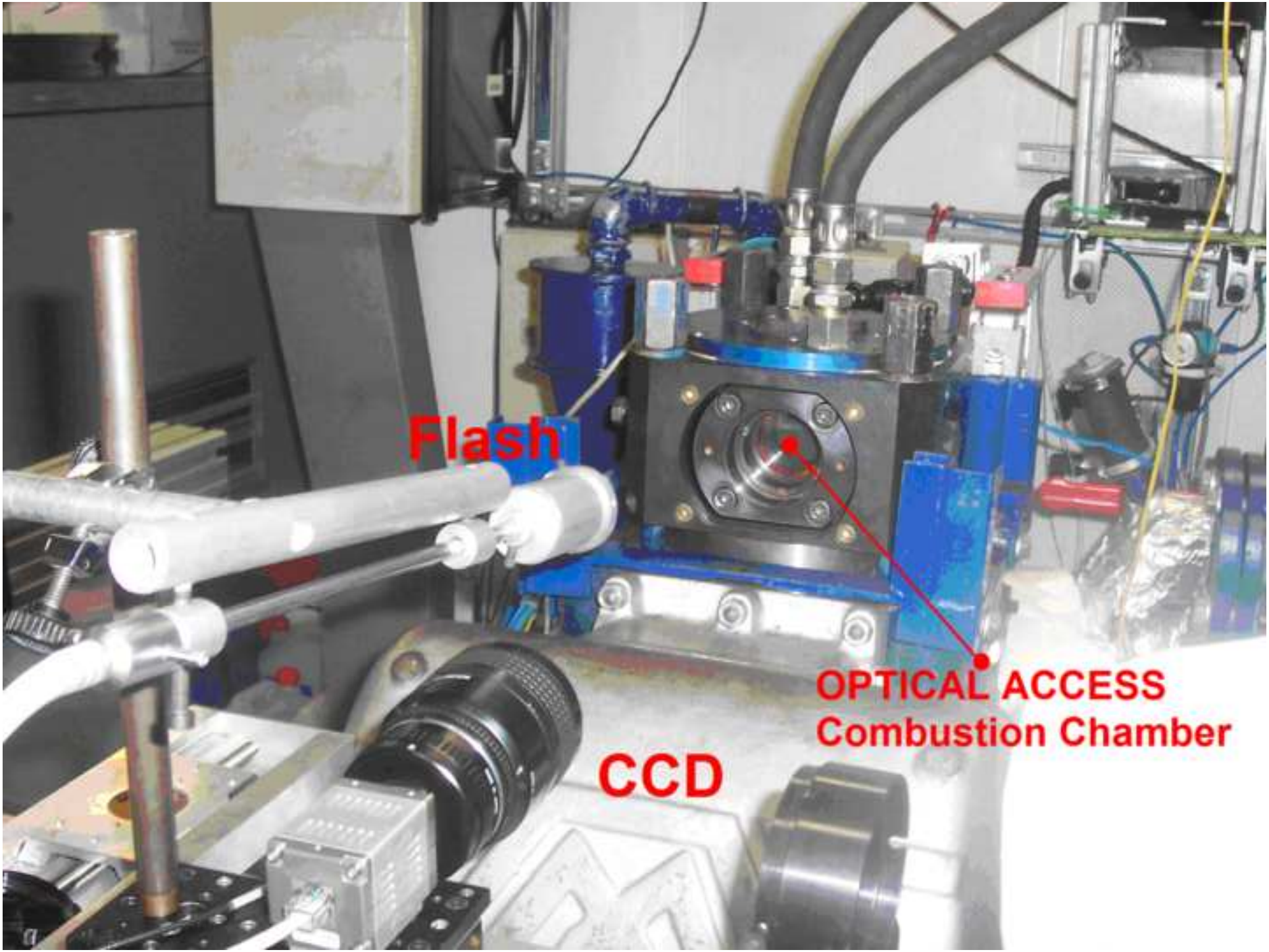

Figure 2

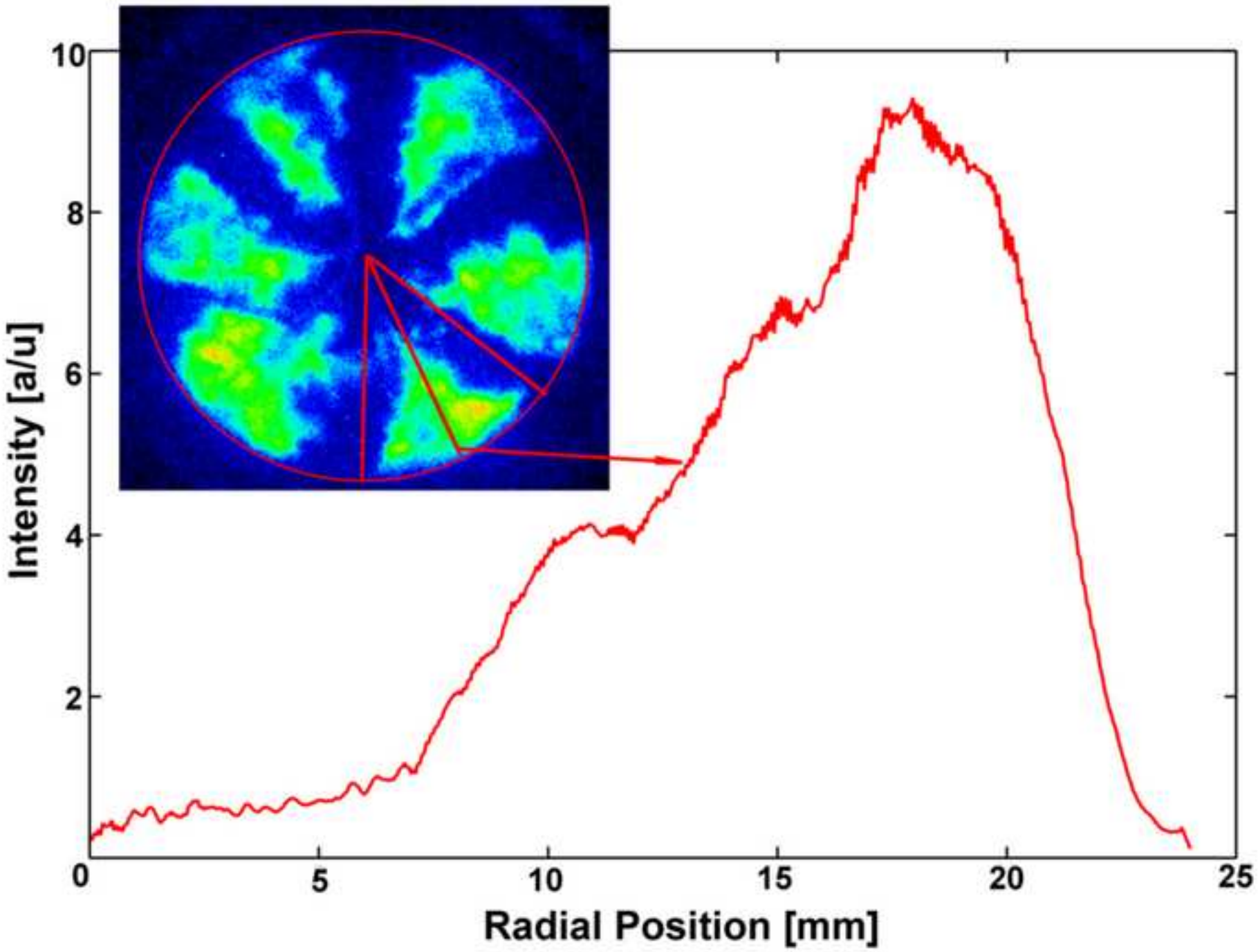

Figure 3

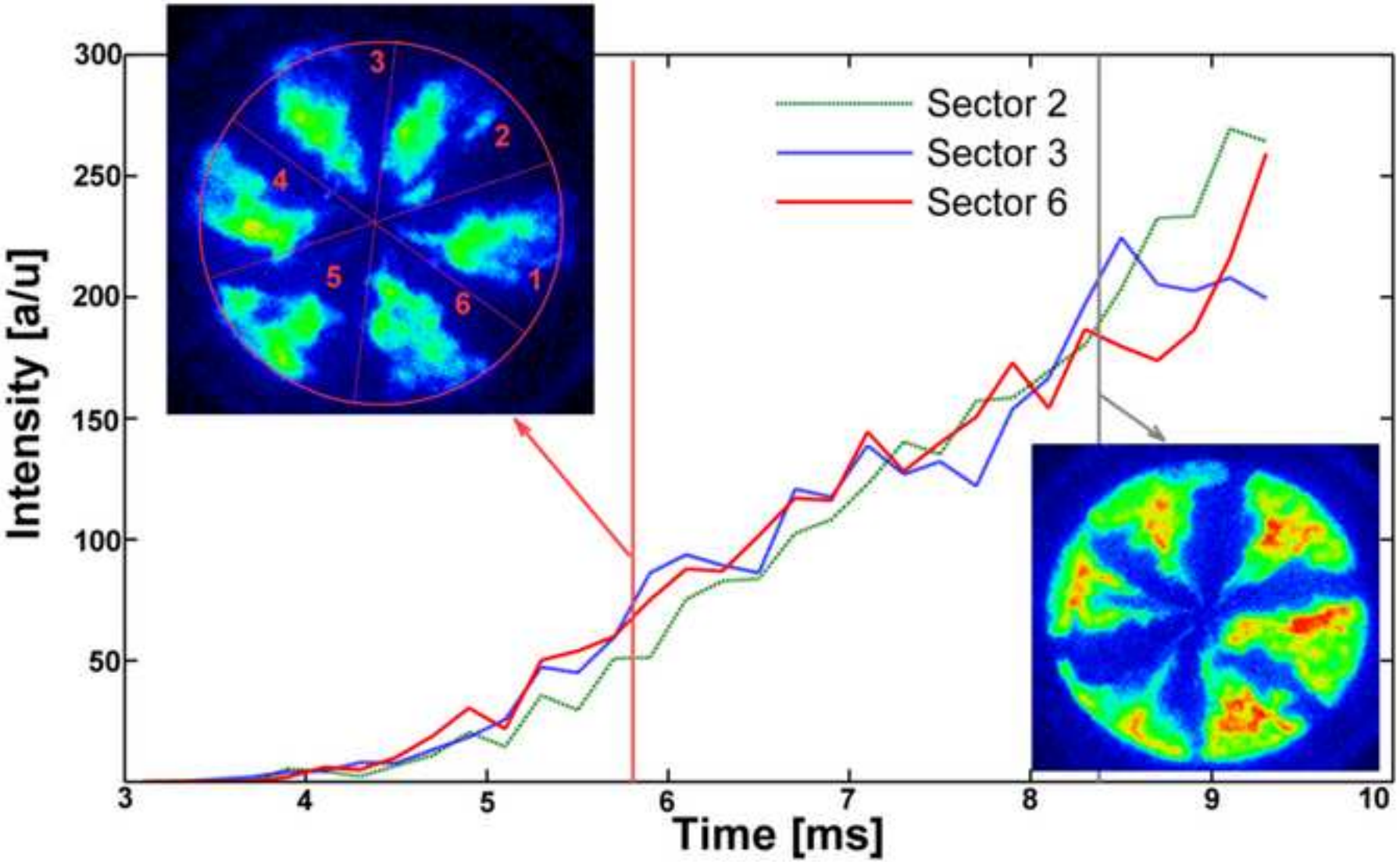
Sector 2
Sector 3
Sector 6
Intensity [a/u]
Time [ms]
300
250
200
150
100
50
3
4
5
6
7
8
9
10
1
2
3
4
5
6

Figure 4

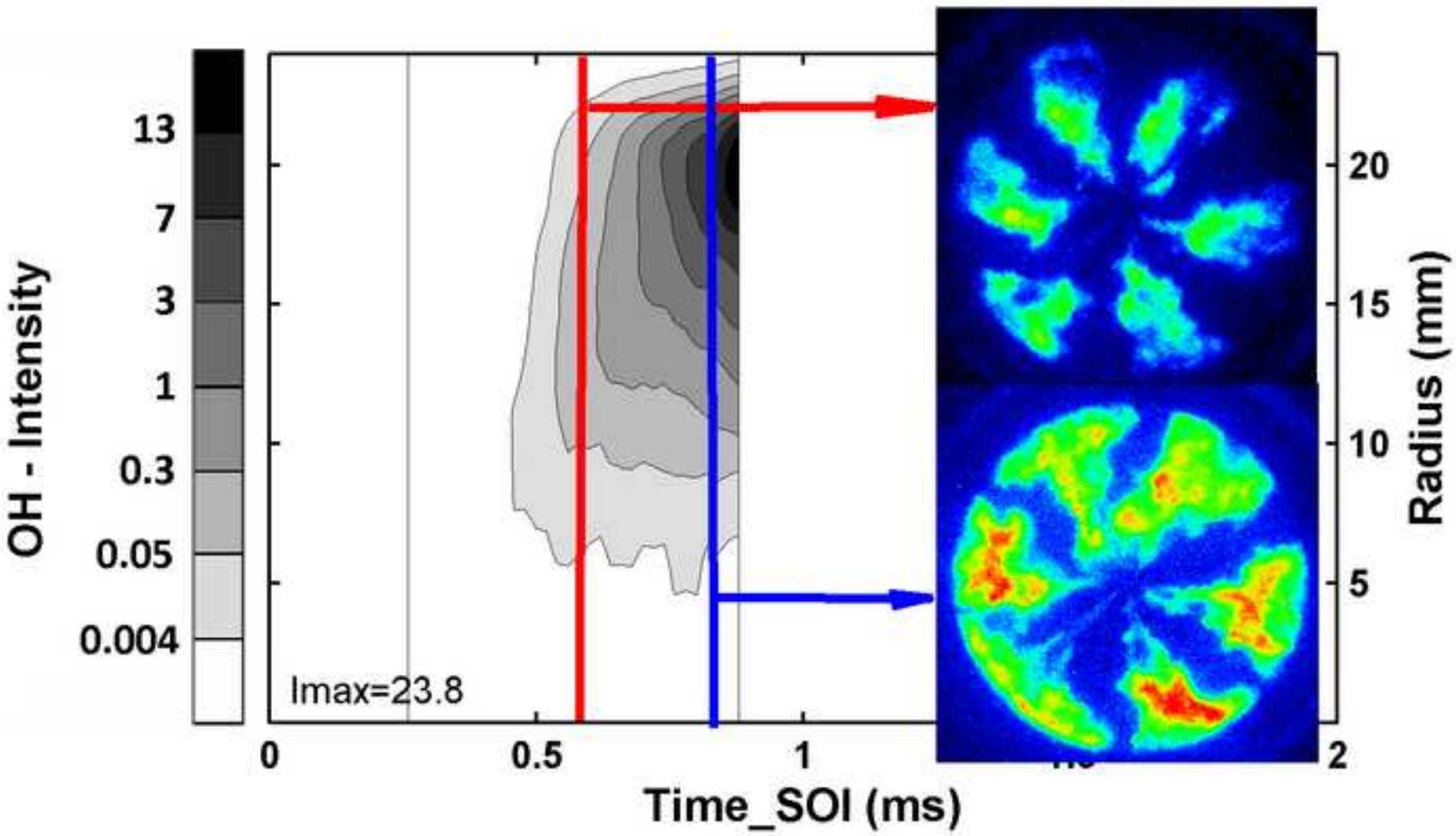
OH - Intensity
13
7
3
1
0.3
0.05
0.004
Imax=23.8
0
0.5
1
2
Time_SOI (ms)
20
15
10
5
Radius (mm)

Figure 5

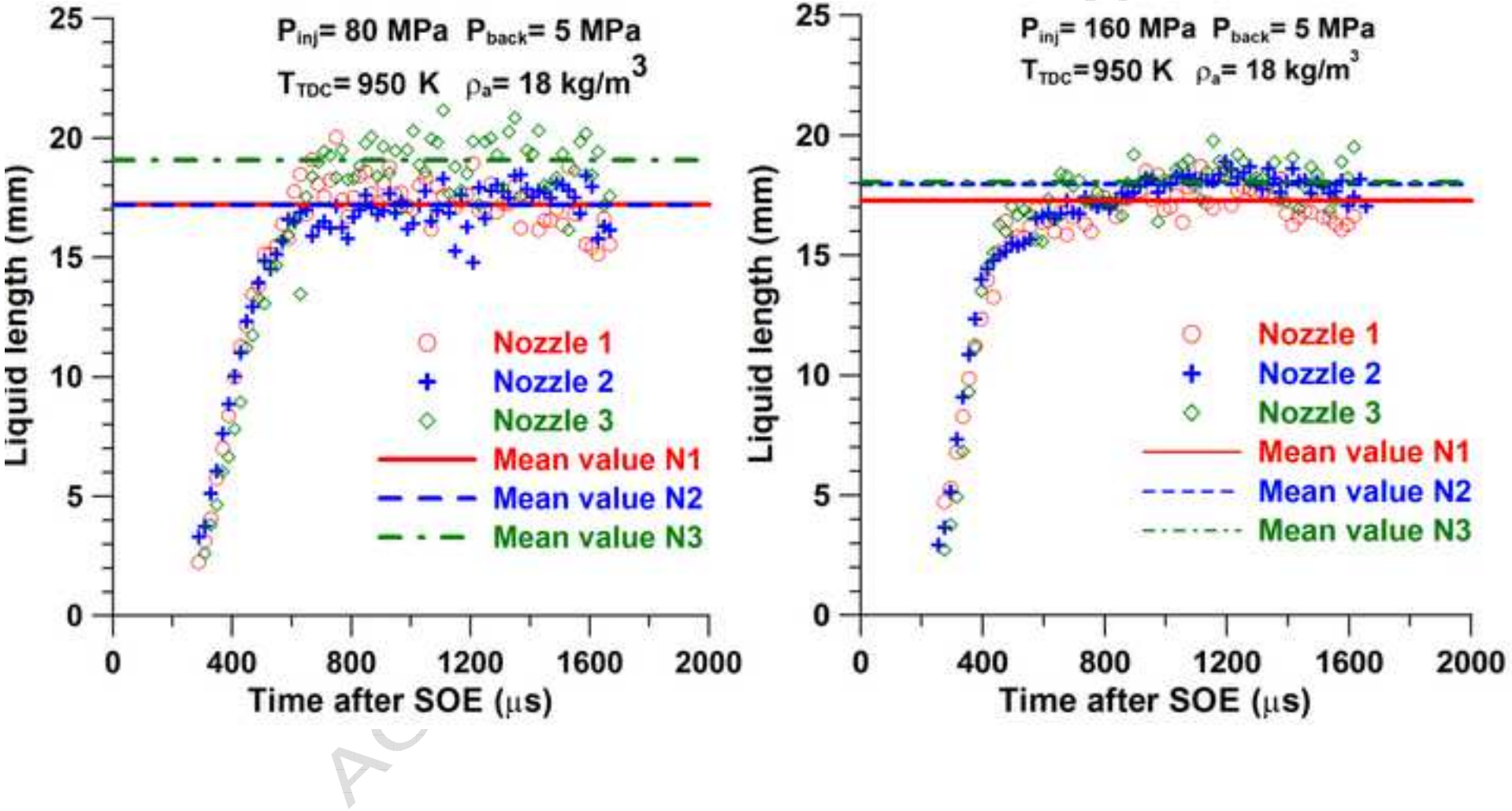
P_inj= 80 MPa P_back= 5 MPa
T_TDC= 950 K ρ_a= 18 kg/m^3
Liquid length (mm)
Time after SOE (μs)
Nozzle 1
Nozzle 2
Nozzle 3
Mean value N1
Mean value N2
Mean value N3
P_inj= 160 MPa P_back= 5 MPa
T_TDC=950 K ρ_a= 18 kg/m^3
Liquid length (mm)
Time after SOE (μs)
Nozzle 1
Nozzle 2
Nozzle 3
Mean value N1
Mean value N2
Mean value N3

Figure 6

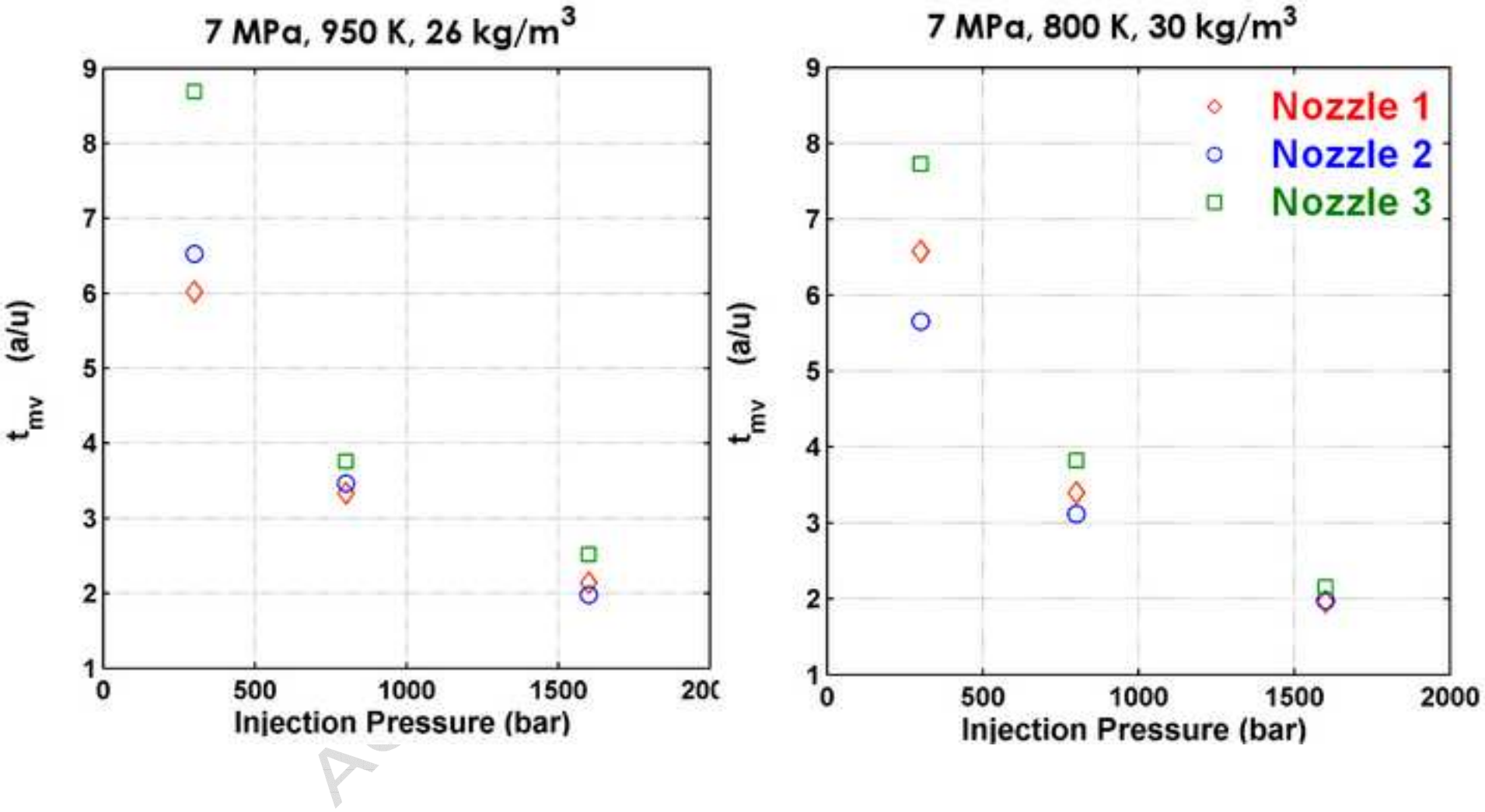
7 MPa, 950 K, 26 kg/m3
7 MPa, 800 K, 30 kg/m3
Nozzle 1
Nozzle 2
Nozzle 3
t_mv (a/u)
Injection Pressure (bar)
0
500
1000
1500
2000
1
2
3
4
5
6
7
8
9

Figure 7

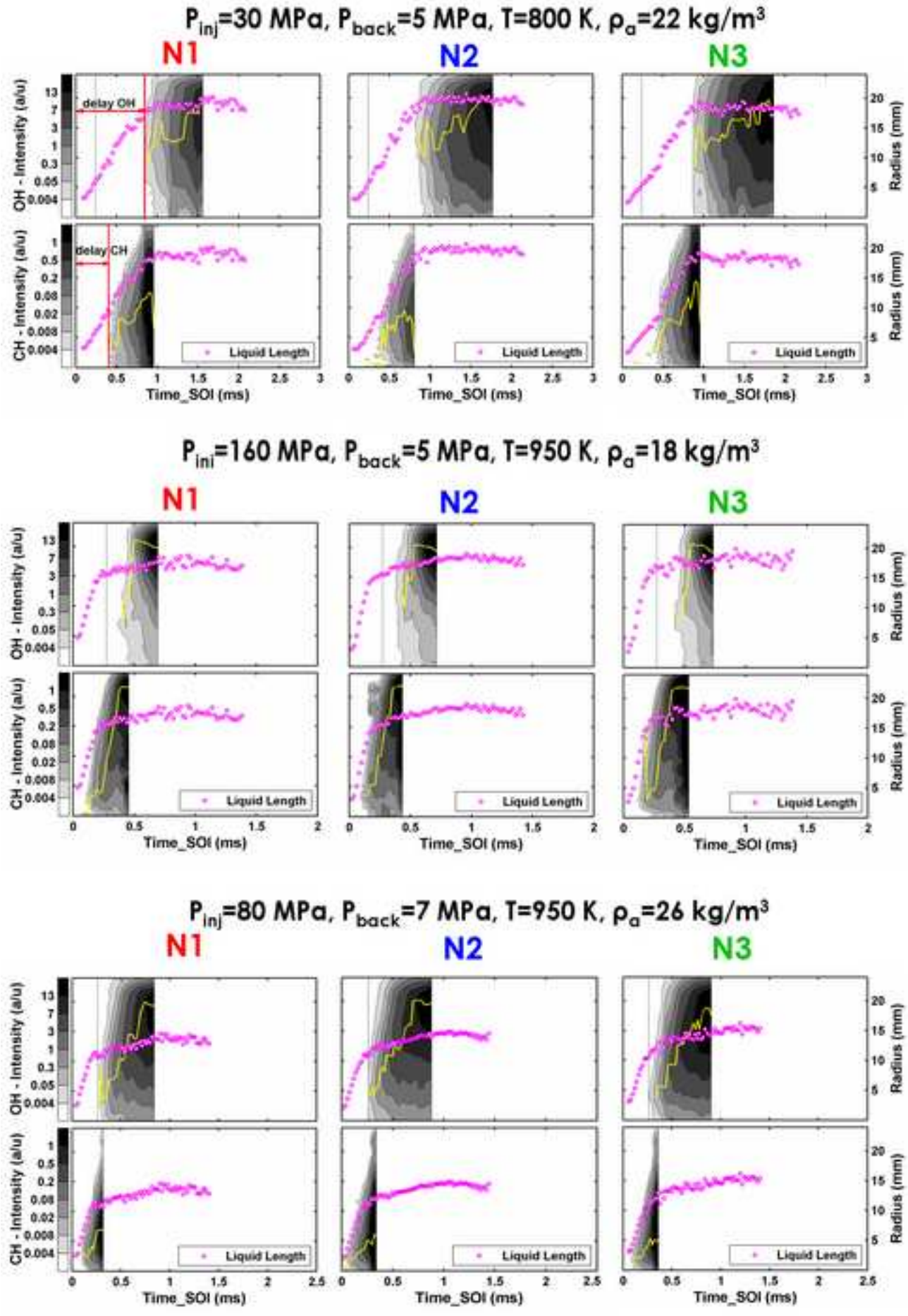

Figure 8

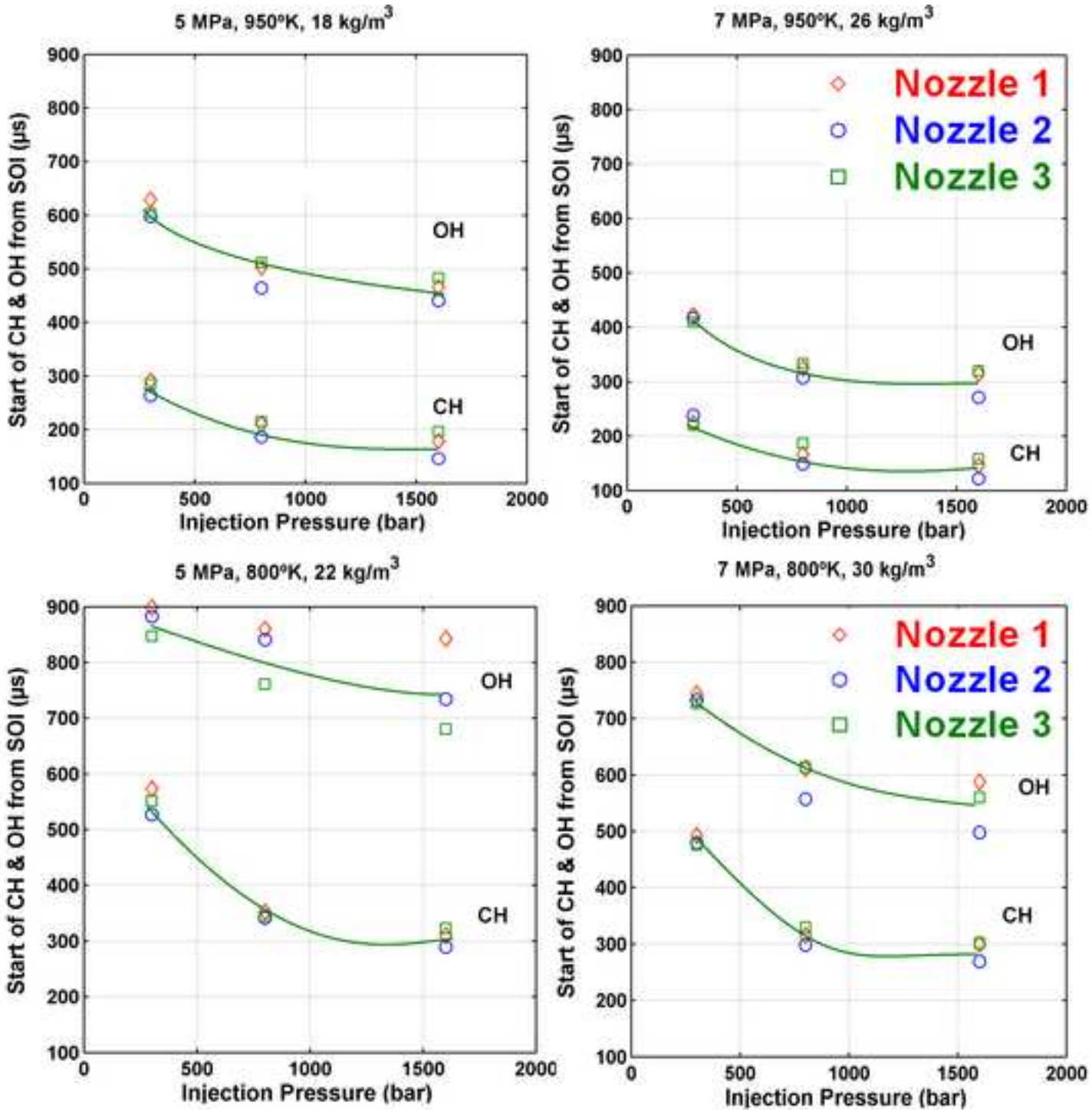

Figure 9

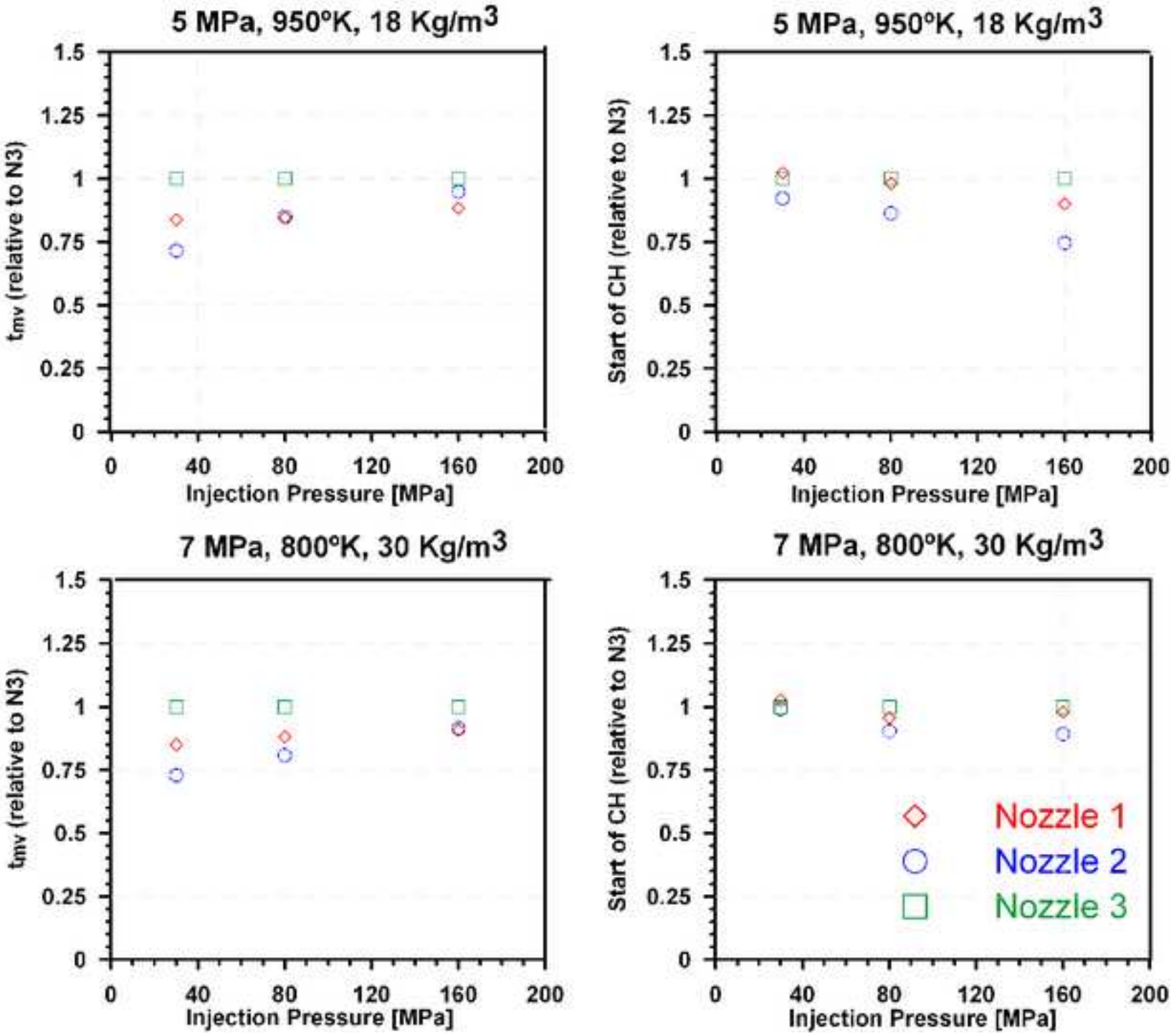
5 MPa, 950°K, 18 Kg/m3
tmv (relative to N3)
Injection Pressure [MPa]
5 MPa, 950°K, 18 Kg/m3
Start of CH (relative to N3)
Injection Pressure [MPa]
7 MPa, 800°K, 30 Kg/m3
tmv (relative to N3)
Injection Pressure [MPa]
7 MPa, 800°K, 30 Kg/m3
Start of CH (relative to N3)
Injection Pressure [MPa]
Nozzle 1
Nozzle 2
Nozzle 3

Figure 10

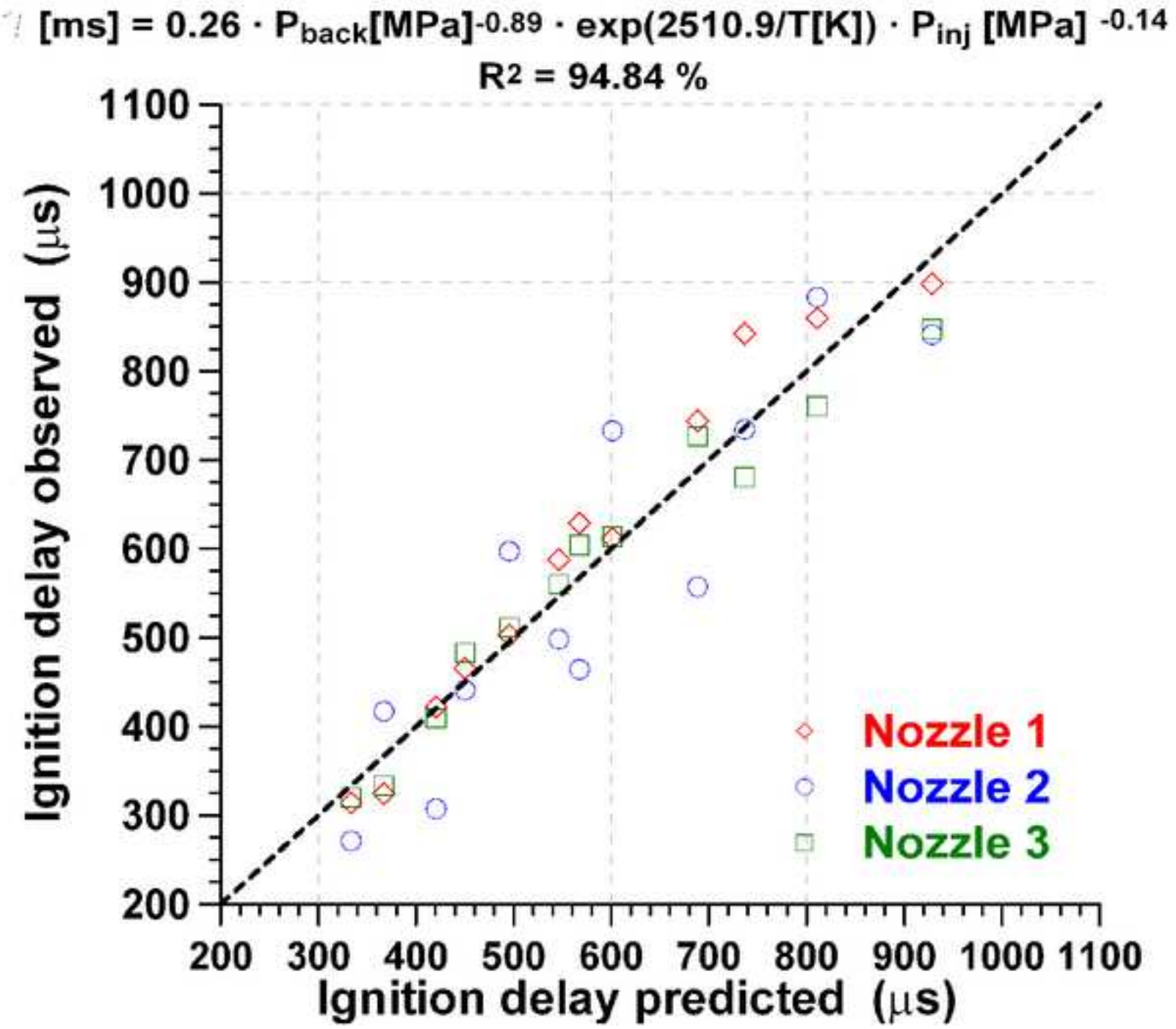
[ms] = 0.26 · P_back[MPa]^-0.89 · exp(2510.9/T[K]) · P_inj [MPa]^-0.14
R² = 94.84 %
Ignition delay observed (μs)
Ignition delay predicted (μs)
200
300
400
500
600
700
800
900
1000
1100
Nozzle 1
Nozzle 2
Nozzle 3